NUMERICAL INVESTIGATIONS ON TWO-PHASE FLOW MODES IN EVAPORATIVE CONDENSERS

Maria Fiorentino, Giuseppe Starace*

Department of Engineering for Innovation, University of Salento, Via per Monteroni, Lecce, 73100, Italy

***Corresponding author.**

E-mail addresses: maria.fiorentino@unisalento.it (M. Fiorentino), giuseppe.starace@unisalento.it (G. Starace)

Keywords: Falling film evaporation, Flow modes, Evaporative condensers

Abstract

Falling film evaporation over horizontal tubes consists of simultaneous heat and mass transfer processes: in evaporative condenser it improves the heat rejection from the condensing refrigerant to the air.

The liquid flow is generally influenced by viscous, gravity, tension effects, liquid mass flow rate, tube diameter and spacing and distance from the feeding system.

In this work, a two-dimensional numerical model of the falling film evaporation on horizontal tubes is presented. The temporal change characteristics of the film flow process were studied and different types of flow (stable film and drops modes) were investigated, by varying the ratio between the water-to-air mass flow ratio.

The effect of the tubes arrangement on the flow mode was analyzed too: an increase of 73 % of the longitudinal pitch corresponds to an increase of 66.7 % of the minimum water mass flow rate that prevents the film break-up.

The tradeoff curve for a given geometry was obtained: at a specific air mass flow rate the transition from the stable film to the drops mode condition (and vice versa) occurs in the uncertainty zone, whose amplitude refers to a water mass flow rate variation set to 10%.

Nomenclature

$A_{interface}$	Interfacial area density, (m^{-1})
Ar	Archimedes number, (-)
C	Empirical constant, (-)
d_{ext}	Tube outer diameter, (mm)
d_p	Primary drop diameter, (m)
D_{wa}	Water vapor diffusion coefficient to air, ($m^2\ s^{-1}$)

E	Energy source, ($W \cdot m^{-3}$)
f	Friction factor, (-)
F	Volume force, ($N \cdot m^{-3}$)
g	Gravitational acceleration ($m \cdot s^{-2}$)
G_M	Surface molar velocity of air, ($kg \cdot mole \cdot m^{-2}\ s^{-1}$)
Ga	Galileo number, (-)
H	Enthalpy, ($J \cdot kg^{-1}$)
$i_{vap,w}$	Heat of vaporization of water, ($J \cdot kg^{-1}$)
k_{eff}	Effective thermal conductivity, ($W \cdot m^{-1}K^{-1}$)
k_G	Molar transfer coefficient,($kg \cdot mole \cdot Pa^{-1} \cdot m^{-2}s^{-1}$)
k_m	Mass transfer coefficient from liquid water to vapor, ($kg \cdot m^{-3}s^{-1}$)
K	Coefficient corresponding to the different flow modes, (-)
$\dot{m}$	Mass flow rate, ($kg \cdot s^{-1}$)
M	Molecular weight, ($kg \cdot kmol^{-1}$)
N_A	Water molar flux, ($kg \cdot mole \cdot m^{-2}s^{-1}$)
N_R	Number of rows,(-)
p	Pressure, (Pa)
P	Pitch, (mm)
Re	Reynolds number, (-)
S	Energy source term, ($W \cdot m^{-3}$)
Sc	Schmidt number, (-)
t	Time, (s)
T	Temperature, (K)
v	Velocity, ($m \cdot s^{-1}$)
x	Specific humidity, ($kg \cdot kg_{d,a}{}^{-1}$)

Greek symbols

α	Volume fraction, (-)
Γ	Water mass flow rate over half tube per unit length, ($kg \cdot m^{-1}s^{-1}$)
Δ	Difference
δ	Water film thickness, (mm)
θ	Angular coordinate around the tube, (°)
λ	Stability wavelength on horizontal tubes, (m)
μ	Dynamic viscosity, ($Pa \cdot s$)

ρ	Density, (kg·m^{-3})
σ	Water surface tension, (N·m^{-1})
χ	Correction factor, (-)

Subscripts

atm	Atmospheric
d,a	Dry air
l	Longitudinal
m,a	Moist air
max	Maximum
sat	Saturation
t	Transversal
$trans$	Stable film-drops mode transition
v	Water vapor
w	Water
$wall$	Wall

1. Introduction

Due to its interest in many fields (chemical and food industries, refrigeration equipment and so on), many researchers in the past have investigated the falling film evaporation over horizontal tubes, that involves simultaneous and complex heat and mass transfer processes. When carried out in evaporative condensers it improves the heat rejection from the condensing refrigerant to the air.

Chyu [1] computed the film thickness at any angular position θ as function of the flow rate over half a tube of unit length, water and air density and water dynamic viscosity:

$$\delta = \left[\frac{3\mu_w \Gamma}{g\rho_w(\rho_w - \rho_{m,a})\sin\theta}\right]^{1/3} \quad (1)$$

Rogers [2] calculated the laminar film thickness on horizontal tubes as function of the film Reynolds and Archimedes numbers, solving the motion and energy equations. The film Reynolds number is expressed as function of the water flow rate over half a tube per unit length:

$$Re_w = \frac{4\Gamma}{\mu_w} \quad (2)$$

The Archimedes number is:

$$Ar = \frac{g\rho_w{}^2 d_{ext}{}^3}{\mu_w{}^2} \tag{3}$$

Then he obtained an empirical relationship for the film thickness [3]:

$$\delta = 1.186\left(\frac{Re_w}{Ar}\right)^{1/3} \tag{4}$$

Armbruster et al. [4] investigated the falling film flow mode transitions for plain tubes, observing that the flow pattern depends on the film Reynolds number and the tube spacing.

Hu et al. [5] proposed a flow mode transition depending on the relationship between the film Reynolds number and the Galileo number. The Galileo number is defined as:

$$Ga = \frac{\rho_w \sigma^3}{g\mu_w{}^4} \tag{5}$$

At each relationship between these two dimensionless quantities corresponds a different flow mode.

Yung et al. [6] expressed the mass flow rate per unit length at the stable film-drops mode transition as:

$$\Gamma_{trans} = 0.81\frac{\rho_w}{\lambda}\frac{\pi d_p{}^3}{6}\left(\frac{2\pi\sigma}{\rho_w\lambda^3}\right)^{1/2} \tag{6}$$

λ is the stability wavelength on horizontal tubes and d_p is the diameter of the primary drop written as:

$$d_p = C\sqrt{\frac{\sigma}{g\rho_w}} \tag{7}$$

The empirical constant for water C is equal to 3. Honda et al. [7] defined a coefficient K as follows, whose value range corresponds to different flow modes:

$$K = \frac{\Gamma}{\sigma^{3/4}}\left(\frac{g}{\rho_w}\right)^{1/4} \tag{8}$$

All the cited works were focused on the falling film evaporation in still air. Actually in the previous empirical correlations no dependence on the air velocity was present, while the influence on the flow formation and heat transfer has a great interest in real evaporative condenser configuration, where water falls down against a countercurrent air flow provided by a fan.

The authors who dealt with the modeling of evaporative condensers and cooling towers aimed to evaluate the thermal performance of the whole system.

Parker and Treybal [8] suggested a design method for countercurrent evaporative coolers, based on Merkel hypothesis (Lewis number equal to unity). They took into account the water temperature variation in the heat transfer process, while previous authors referred to a constant mean value.

Mizushina [9] experimentally studied evaporative coolers and obtained empirical correlations for heat and mass transfer coefficients.

Kreid [10], Leidenforst and Korenic [11] focused on finned evaporative condensers.

Bykov et al. [12] studied heat and mass transfer as well as fluid flow characteristics in evaporative condensers. They detected three different zones: a. the area above the tube bundle b. the tube bundle c. the area between the coil and the bottom sump; they investigated on water temperature and air enthalpy changes depending on the elevation above the sump level.

Webb [13] developed a unified mathematical model for cooling towers, evaporative coolers and condensers.

Dreyer et al. [14] studied evaporative coolers and condensers and compared empirical correlations provided by different authors to determine heat and mass transfer coefficients. They observed that expressions obtained by Mizushina [9] were valid over a wider range of operating conditions.

Zalewski and Gryglaszewski [15] developed a mathematical model based on analysis carried out by Poppe et al. [16]. They applied expression suggested by Bykov [12] for the heat transfer coefficient and modified the expression suggested by Bosnjakovic and Blackshear [17] for the mass transfer coefficient with a correction factor.

Ettouney et al. [18] investigated on evaporative condensers performance by varying the condensing temperature and the water to air mass flow rates ratio.

Qureshi and Zubair [19] carried out a study on the influence of fouling in evaporative coolers and condensers performance. In order to predict the device behavior, they used the model developed by Dreyer [14] adding the fouling factor.

Then Qureshi and Zubair [20] obtained an empirical relationship to evaluate water evaporation rate and observed a maximum deviation of 2% between calculated and experimental values.

In the most recent works the phenomena involved in evaporative condensers were modeled at the tube scale.

Jahangeer and Tay [21] developed a model using finite difference technique, to simulate a single straight tube wet by the water film and invested by air in a cross flow scheme.

They studied the influence of many boundary conditions, like condensing temperature, dry air bulb temperature and relative humidity on heat transfer coefficient.

In [22] the evaporative condenser at tube scale was modeled with Fluent under stable film condition and the computed overall heat transfer coefficients values compared with those coming from empirical relationships.

Islam and Jahangeer [23] carried out experimental and theoretical analyses on an evaporatively cooled bare tube condenser: a good agreement between experimental and numerical results was obtained.

In this work, the different flow modes as influenced by the working fluids mass flow rates values are shown as a result of numerical investigations on the falling film evaporation phenomenon over horizontal tubes.

2. Mathematical model

Evaporative condenser geometry consists in staggered straight tubes, whose outer surface is wet by a liquid film while air flows in a countercurrent configuration.

The computational domain was set to represent the portion of fluid between two staggered tubes whose horizontal and vertical distances are equal to half of the transversal and to the longitudinal pitch, respectively. The geometry characteristics are summarized in Table 1 and the computational domain with the boundary conditions are shown in Figure 1.

Table 1. Geometrical parameters of the tube banks.

Figure 1. Computational domain and boundary conditions.

The model is based on the following assumptions:

I. The refrigerant condenses inside the tubes, and causes a nearly constant wall temperature (in the boundary condition setting, small temperature differences on the tube outer walls were neglected).

II. The air conditions at a specific distance from the inlet section were assumed the same over the tube length (i.e. along the z-direction); thus the problem became two-dimensional.

III. Since air and water flows have the same direction (are not crossed) and has been assumed that water hasn't preferential directions, but is equally distributed by a feeding system, a symmetric boundary condition was applied to the vertical surfaces of the computational domain.

At the water inlet, the liquid mass flow rate was imposed falling directly on the tube upper quadrant. At the air inlet and outlet the gauge pressures were specified: the pressure drop was set to determine the air mass flow rate.

The relationship between the pressure drop and the air velocity is [24]:

$$\Delta p = N_R \cdot f \cdot \chi \cdot \frac{\rho_{m,a} {v_{m,a\,max}}^2}{2} \tag{9}$$

The correction factor takes into account the effects of deviation from equilateral arrangement.

At the solid surfaces a no-slip wall boundary condition was adopted with a constant temperature, while the remaining surfaces were considered symmetric, since no reason for preferential directions of the water could be taken into account.

The continuity, momentum and energy equations were solved using the CFD code Ansys Fluent (Release 14.5).

$$\frac{\partial}{\partial t}(\rho\vec{v}) + \nabla \cdot (\rho\vec{v}\vec{v}) = -\nabla p + \nabla \cdot [\mu(\nabla\vec{v} + \nabla\vec{v}^T)] + \rho\vec{g} + \vec{F} \tag{10}$$

$$\frac{\partial}{\partial t}(\rho H) + \nabla \cdot \left(\vec{v}(\rho H)\right) = \nabla \cdot \left(k_{eff}\nabla \mathrm{T}\right) + \mathrm{S} \tag{11}$$

The multiphase model Volume of Fluid was adopted. The VOF method is used to track the position of the interface between the two phases (water and moist air), where the heat and mass transfer phenomena occur.

A scalar value, called "volume fraction" is computed in each computational cell: it represents the area portion of the cell occupied by the phase.

The volume fractions of all the phases sum up to unity.

If the cell volume fraction of the water is denoted as α_w three conditions are possible:

- $\alpha_w = 0$: the cell is filled with moist air.
- $\alpha_w = 1$: the cell is filled with water.
- $0 < \alpha_w < 1$: the cell contains the interface between the two phases.

The water volume fraction of each cell is computed solving the continuity equation:

$$\frac{\partial \alpha_w \rho_w}{\partial t} + \nabla \cdot (\alpha_w \rho_w \vec{v}_w) = \dot{m}_{w,v} \tag{12}$$

Where $\dot{m}_{w,v}$ indicates the mass transfer from water to vapor.

The values of water volume fractions in each cell don't uniquely identify the interface, in fact different interface configurations may correspond to them. Two different techniques for the interface reconstruction are available in Fluent: the donor acceptor and the geometric reconstruction. The geo reconstruction technique tracks the interface through piecewise linear segments and consists of two steps: reconstruction and propagation.

In the reconstruction step the position of the linear interface relative to the center of each partially filled cell is computed and it's approximated by a straight line with a slope determined from the unit

normal vector to the segment. The normal to the segment and the cell phase volume fraction uniquely determine the linear interface in the cell.

During the second step the interface motion is obtained by the knowledge of the normal and tangential velocity distribution at the interface and the amount of advection fluid through it. Then the volume fraction in each cell of the computational domain is derived by the balance of fluid mass fluxes.

Figure 2. Example of interface representation.

As the initial condition, the computational domain was set to be filled with air.

The moist air was modeled as a mixture of dry air and water vapor species.

A routine written in C (the User Defined Function) was loaded into the solver in order to:

- Customize the thermo-physical properties of the moist air.
- Compute the mass transfer coefficient from liquid water to water vapor, that allows to model the water vaporization.

The mass transfer coefficient was determined as follows:

Water vapor diffusion coefficient was obtained using the regression curve fit to the data [25].

$$D_{wa} = 10^{-6}\left(-2.775 + 4.479 \cdot 10^{-2} T_{m,a} + 1.656 \cdot 10^{-4} T_{m,a}^{2}\right) \quad (13)$$

The Schmidt number could be computed as:

$$Sc = \frac{\mu_{m,a}}{\rho_{m,a} D_{wa}} \quad (14)$$

The surface molar velocity of air depends on the air density, velocity and molecular weight:

$$G_M = \frac{v_{m,a} \rho_{m,a}}{M_{m,a}} \quad (15)$$

$$M_{m,a} = \frac{M_{d,a}}{1 + 0.608 \cdot x_{m,a}} \quad (16)$$

The molar transfer coefficient was defined as:

$$k_G = \frac{0.281 Re_{m,a}^{-0.4} G_M}{p_{atm} Sc^{0.56}} \quad (17)$$

The water molar flux is proportional to the difference between saturation pressure at liquid water temperature and water vapor pressure in the air surrounding the tube.

$$N_A = k_G (p_{v,sat} - p_v) \quad (18)$$

$$p_{v,sat} = \exp(65.81 - \frac{7066.27}{T_w} - 5.976 \ln T_w) \quad (19)$$

$$p_v = \frac{(x_{m,a} \cdot p_{atm})}{(0.622 + x_{m,a})} \quad (20)$$

The mass transfer coefficient represents the vaporized mass flow rate per unit volume:

$$k_m = N_A M_{m,a} A_{interface} \quad (21)$$

The Interfacial Area Density is the interfacial area between liquid and gas per unit mixture volume and was determined through the User Defined Function.

The knowledge of the mass transfer coefficient and the water specific enthalpy of vaporization allowed to evaluate the latent heat due to water vaporization corresponding to water temperature:

$$E = k_m i_{vap,w}(T_w) \quad (22)$$

3. Grid

The geometry and the grid were generated in Gambit V. 2.3.16.

Unstructured mesh of triangular elements was used with a Pave scheme, while the area around the tube walls was finely meshed through boundary layer technique with quadrangular elements, as a higher quality cells is required in this zone in order to observe the water flow around the tube and to better appreciate the liquid film thickness distribution over the tube.

A size function was attached to the tube walls and applied to the whole domain to control the cell size. In fact the grid was refined where the water-air interface was expected and its size was increased with distance from the tube wall. It was specified in Gambit by a starting value, a growth rate and a maximum value.

To study grid independence, three different grids were compared referring to a water and air mass flow rates of 0.55 and 0.25 kg/s, respectively. The different grids have the following characteristics:

- Grid 1: 20232 elements and 13831 nodes.
- Grid 2: 24510 elements and 16146 nodes,
- Grid 3: 26322 elements and 17105 nodes.

The water film thickness (corresponding to a water volume fraction of 0.5) around the tube on the right was evaluated at the angular position of 90°for the different grids.

Table 2. Results for the grid independence.

The adoption of different grids has no significant impact on the simulation results: increasing the number of nodes as previously reported, the percentage variation of the water film thickness is of 1.6 % (for the Grid 2 with respect to the Grid 1) and of 2.4 % (for the Grid 3 with respect to the Grid 2). The Grid 2, whose details are listed in Tab.3, was so selected for this work.

Table 3. Grid details.

Figure 3. The grid adopted for the simulations.

4. Simulation settings

The simulation settings are listed in Table 4.

Table 4. Simulation settings.

5. Water to air mass flow ratio influence on the flow mode

The effect of the water and air mass flow rates on the flow mode was investigated.
In Table 5 the working fluids mass flow rates corresponding to the different testing cases are summarized.

Table 5. Working fluid mass flow rates for the different testing cases.

Figure 4 shows the temporal evolution of the water flow for the testing case A.

Figure 4. Temporal evolution of the characteristics of film flow (Testing case A).

The computational domain is completely filled with air at the initial time; at t=0.03 s the water has not yet reached the tube walls, while at t=0.09 s it falls down around the tube on the right.
At t=1.41 s the liquid film has reached stability and its behavior in the space between two consecutive tubes is similar to a jet mode [26].
It is not simple to measure the liquid film thickness, as the cells inside the interface region have a water volume fraction less than one.
In the literature [27] the film thickness was evaluated as the distance between the tube wall and the cells with a liquid volume fraction equal to 0.5; this value ensures that 95% of the liquid mass flow rate is captured within the film boundary in the fully developed flow region.

The water film thickness so evaluated (water volume fraction of 0.5) has been so plotted in Figure 5.

Figure 5. Film thickness vs angular position (water volume fraction of 0.5 - Testing case A).

The film thickness goes to infinity at the leading edge, then decreases and reaches the minimum value around 90° and finally increases and rises to infinity for angles greater than 150° (close to the trailing edge). The film thickness decreases with the circumferential velocity (that is influenced by the tangential component of the gravity force). In fact the circumferential velocity of water along the tube surface increases from 0 to 90°, reaches the maximum value in the range between 90° and 140°, and then decreases till 180°.The film thickness decreases with the distance from the water feeding system, actually the area averaged value is about 1 mm for the tube closer to the feed point and 0.75 mm for the farther one.

In Figures 6 and 7 the falling water over the cylinders at different times for the testing case B and C, respectively, are shown.

Figure 6. Temporal change characteristics of film flow process (Testing case B).

When the water mass flow rate is reduced to 0.44 kg the condition of stable film is reached, but as can be observed at t=1.41 s the water film thickness is thinner than the testing case A.

In Figure 7, corresponding to a water mass flow rate of 0.33 kg/s, the liquid falls as jet and adheres to the right cylinder, then it separates into drops, as visible at t=1.34 s.

The water mass flow rate is not sufficient to avoid the film rupture, due to the countercurrent air resistance, which reaches 4 m/s in the smaller cross section.

Regarding the tube on the left, the falling film becomes thinner moving away from the feed point and the rupture occurs before it reaches the wall. This can be observed in Figure 8 (where the contour lines with volume fraction of 0.5 are represented), and in particular at t=0.3 s.

Figures 9 and 10 are referred to the testing cases D and E respectively.

In testing case D the liquid spreads on the tubes as a film.

In testing case E the film rupture occurs at 0.25 s before the water reaches the tube on the left and at t=0.45 s after it reaches the tube on the right.

Figure 7. Temporal change characteristics of film flow process (Testing case C).

Figure 9. Film rupture on the left and right cylinders (Testing case B).

Figure 8. Temporal change characteristics of film flow process (Testing case D).

Figure 10. Temporal change characteristics of film flow process (Testing case E).

6. Influence of the tubes arrangement on the flow mode

The influence of the tubes arrangement on the flow mode (at constant air and water mass flow rates) was analyzed. The simulation settings and the geometric characteristics for the testing case F and G are summarized in Table 6.

Table 6. Simulations settings and geometrical parameters.

In the testing case G an equilateral-triangular layout with a transversal pitch of 100 mm was adopted, as shown in Figure 11.

Figure 11. Tubes layout (Testing case G).

The comparison of the water flow patterns between testing cases F and G is shown in Figure 12.

Figure 12. Influence of the tubes arrangement on the flow mode.

The condition of stable film was reached in the testing case F, while it doesn't happen for the testing case G. Actually, being the vertical distance between the tubes higher, the water velocity increases more under the effect of gravity, the film becomes thinner and breaks up.

In the testing case G, different water mass flow rates were set up, keeping constant the air mass flow rate.

The water mass flow rate has been increased until the flow mode appeared as a stable film: the minimum flow rate that ensured this condition was 0.5 kg/s.

7. Trade-off curve

In this work, two different types of flow were analyzed: the stable film, that is a continuous flow and the drops mode that is a discontinuous one.

The drops mode occurs with the reduction of the ratio between the water and air mass flow rates that causes the start of a periodic regime with drop formation and break-up.

This analysis is an important design issue to ensure that the heat transfer area will be completely wet and to avoid the presence of zones with dry tube surfaces.

Simulations with different air and water mass flow rates (summarized in Table 7) were carried out, and this led to identify a trade-off area referred to a specific geometry. Here, the dashed area in Figure 13 represents the uncertainty zone, whose amplitude refers to a water mass flow rate variation set to 10%. At a specific air mass flow rate the transition from the stable film to the drops mode condition (and vice versa) occurs in this area.

It's hard to accurately evaluate the uncertainty range: a multitude of points should be determined, involving a high computational cost and an accurate trend can be validated only experimentally.

To this purpose a test bench has been designed and tests will be carried out in a near future.

Table 7. Fluids mass flow rates for the different cases.

Figure 13. Trade off curve.

8. Conclusions

The object of this work was to simulate the falling film evaporation occurring in evaporative condenser. The modeled geometry consisted in the repeating portion of the flow field between two staggered tubes wet by a water film. Air was flowing in a countercurrent configuration.

Two different flow modes have been found and investigated, i.e. the stable film and drops mode: when the water mass flow rate decreases the countercurrent air causes the rupture of the film and a periodic flow with drops starts.

The effect of the tubes arrangement on the flow mode was analyzed too: an increase of 73 % of the longitudinal pitch corresponds to an increase of 66.7 % of the minimum water mass flow rate that prevents the film break-up.

Simulations with different water and air mass flow rates were run in order to identify a trade-off area for a specific geometry: it separates two zones where the two different flow modes occur and allows the designer to choose the operating conditions ensuring the complete wetting of the heat transfer area.

Further research is needed to fully detect the flow modes, and in particular a three-dimensional CFD analysis could enable to distinguish between drops, jet and sheet modes.

A test facility suited for the developed numerical model check has been designed to carry out experimental analyses.

Pictures

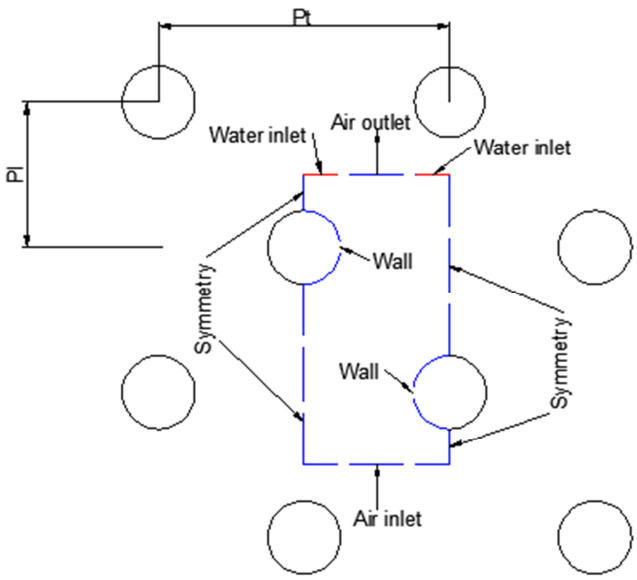

Figure 14. Computational domain and boundary conditions.

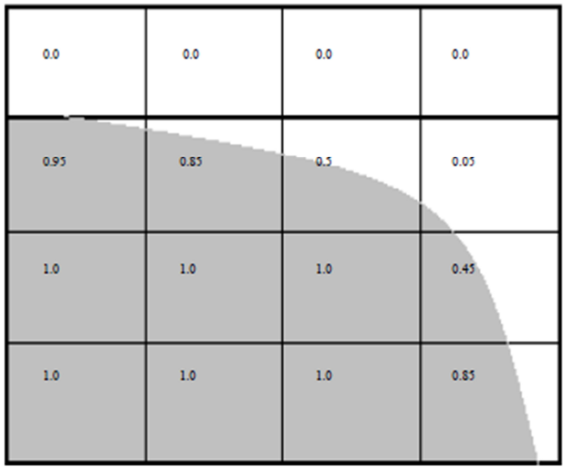

Figure 2. Example of interface representation.

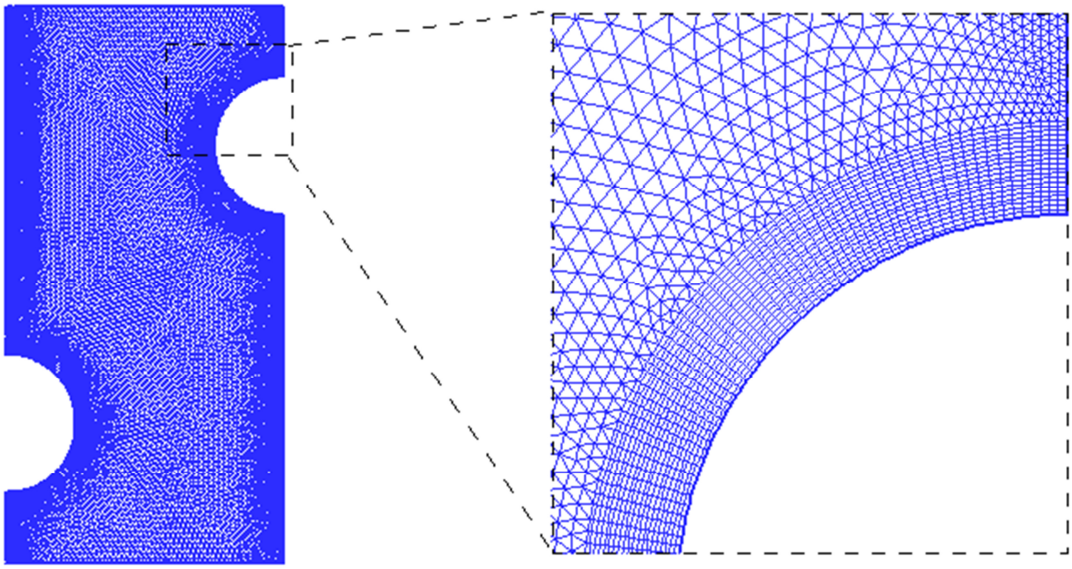

Figure 3. The grid adopted for the simulations.

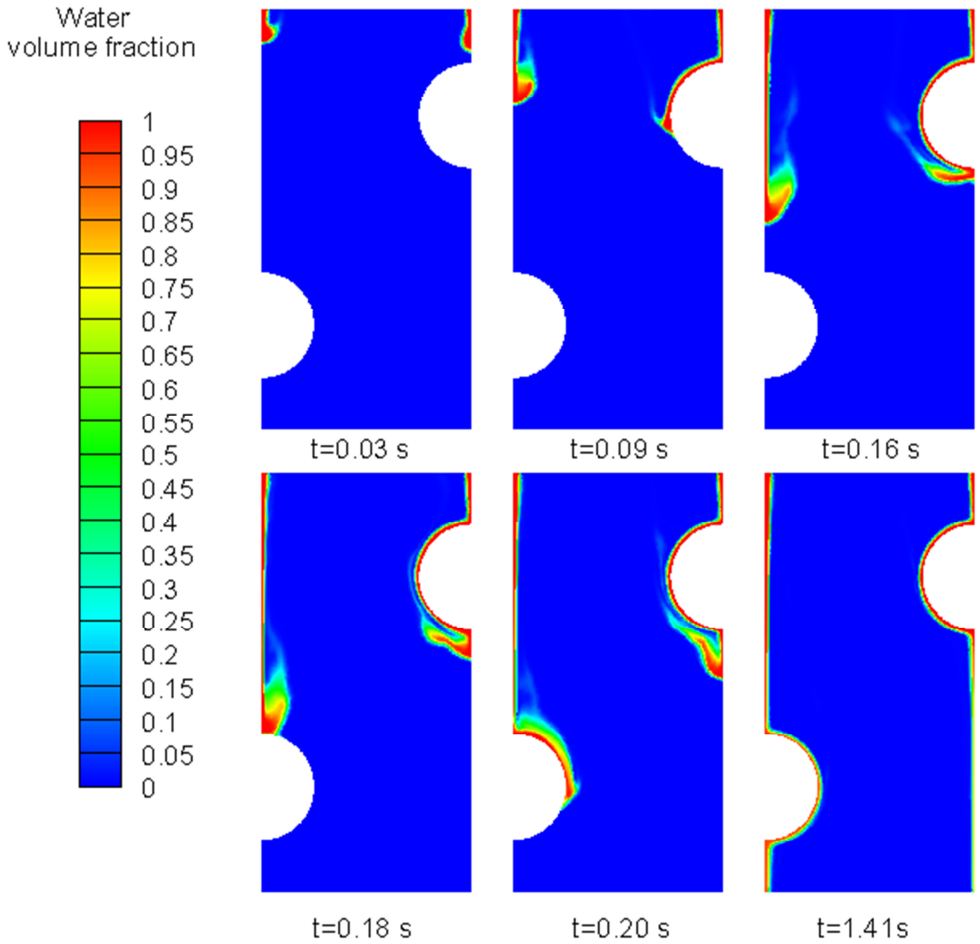

Figure 4. Temporal evolution of the characteristics of film flow (Testing case A).

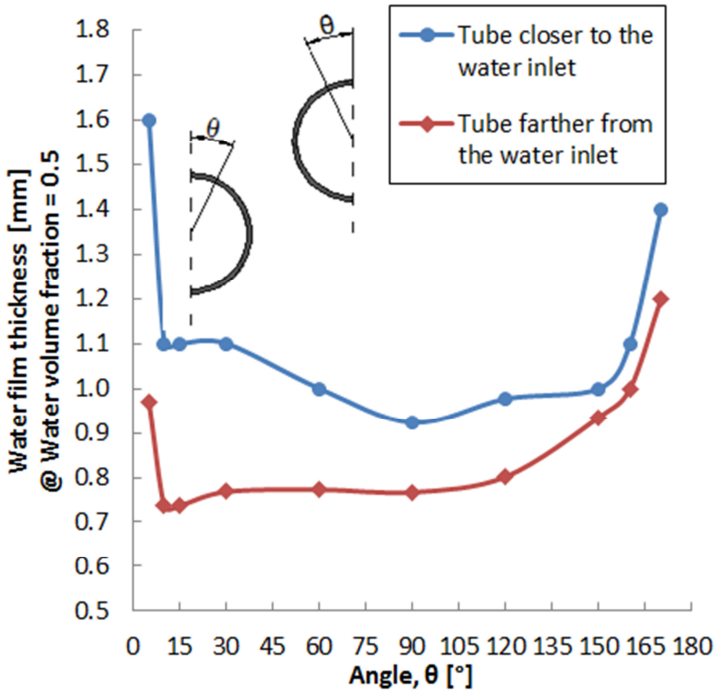

Figure 15. Film thickness vs angular position (water volume fraction of 0.5 - Testing case A).

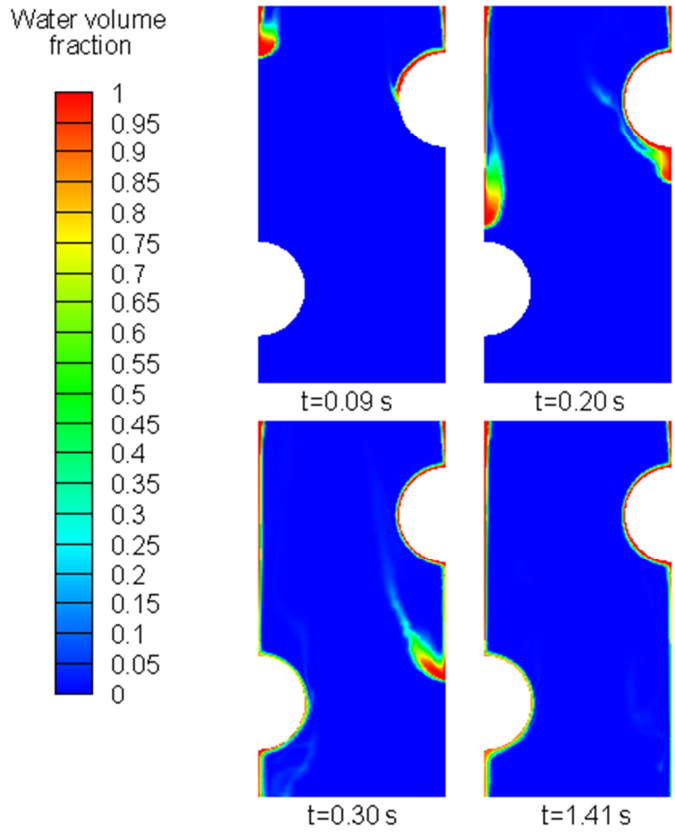

Figure 6. Temporal change characteristics of film flow process (Testing case B).

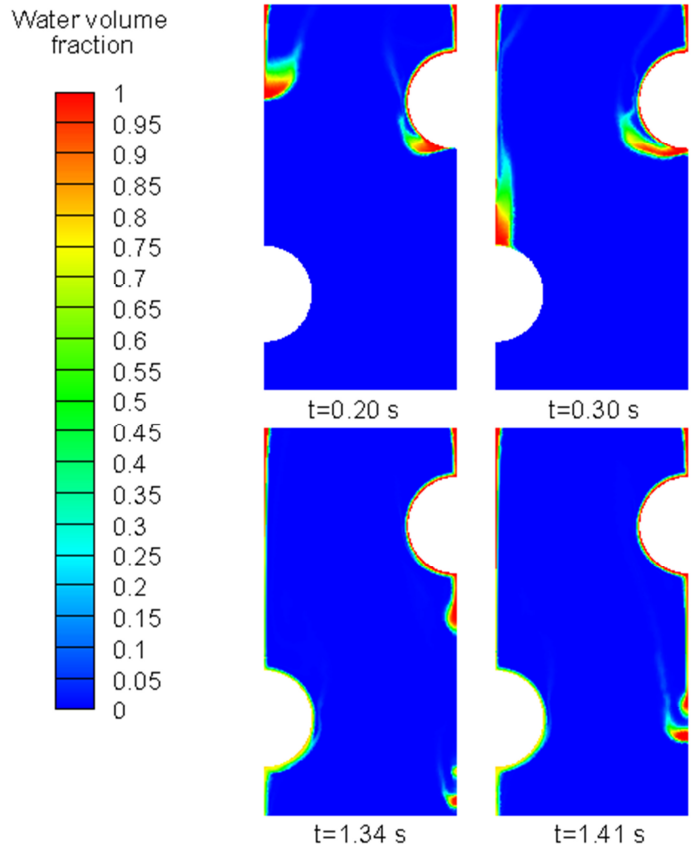

Figure 16. Temporal change characteristics of film flow process (Testing case C).

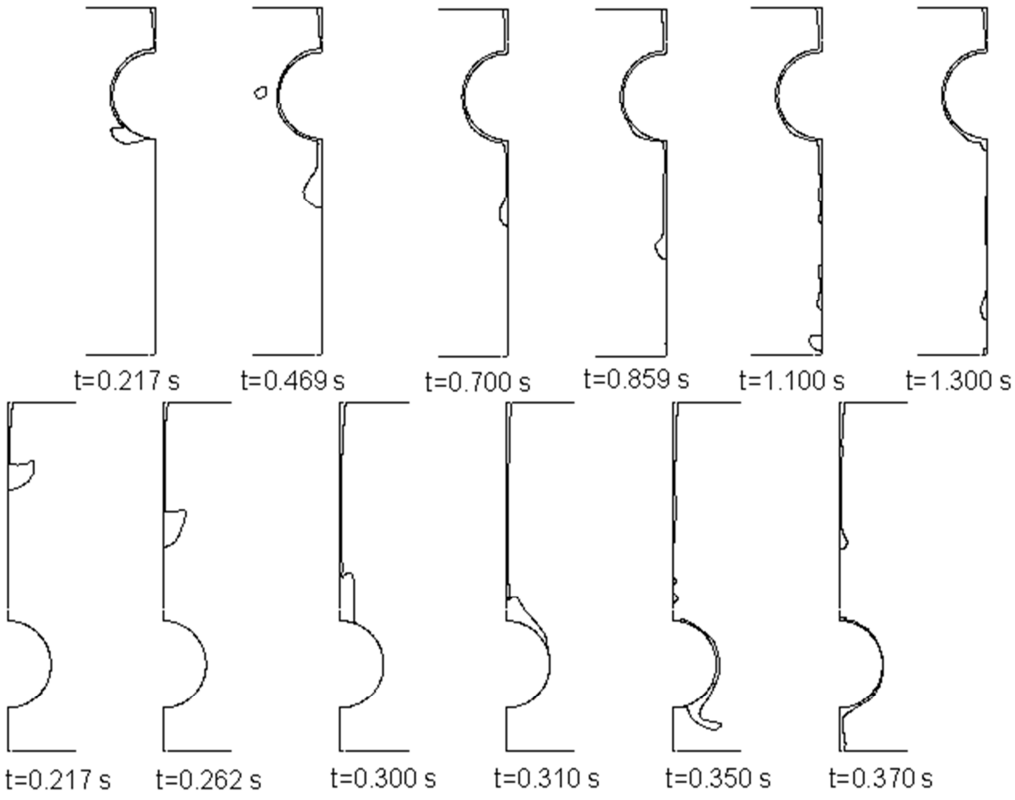

Figure 8. Film rupture on the left and right cylinders (Testing case B).

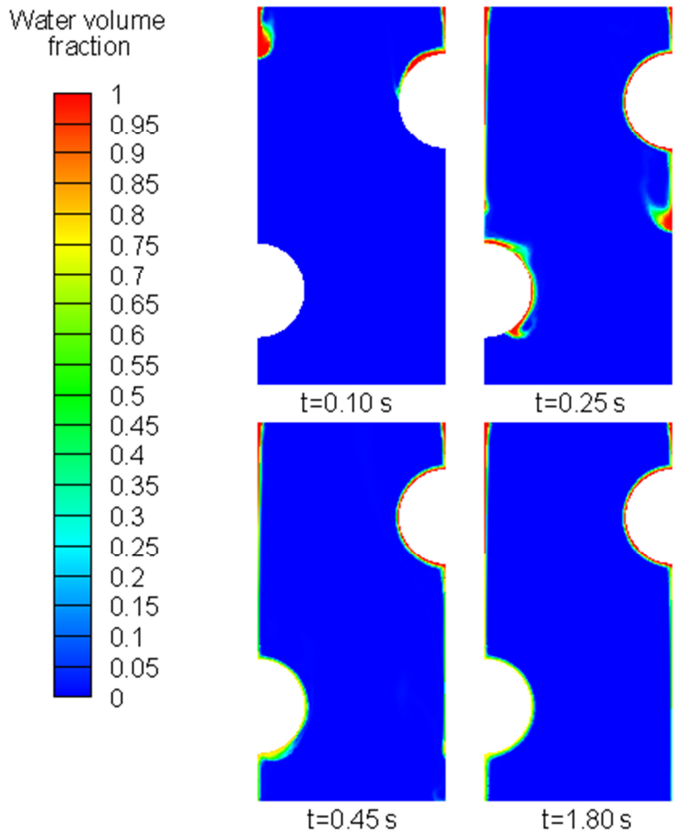

Figure 9. Temporal change characteristics of film flow process (Testing case D).

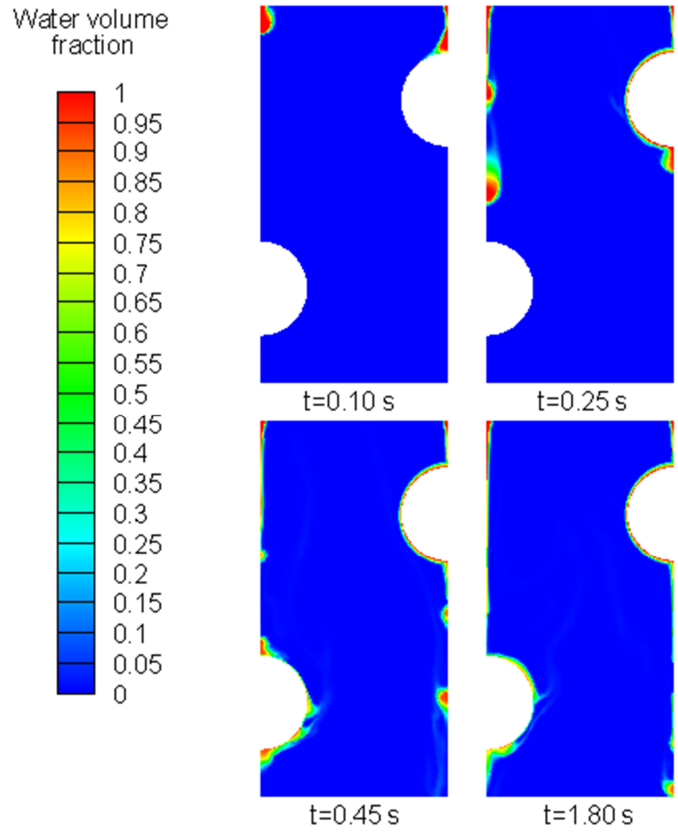

Figure 10. Temporal change characteristics of film flow process (Testing case E).

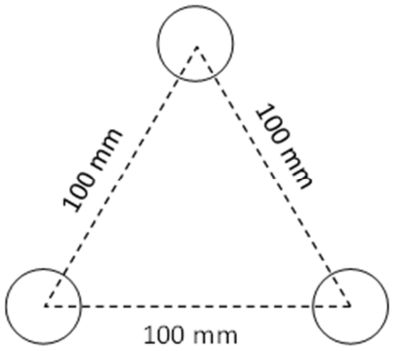

Figure 11. Tubes layout (Testing case G).

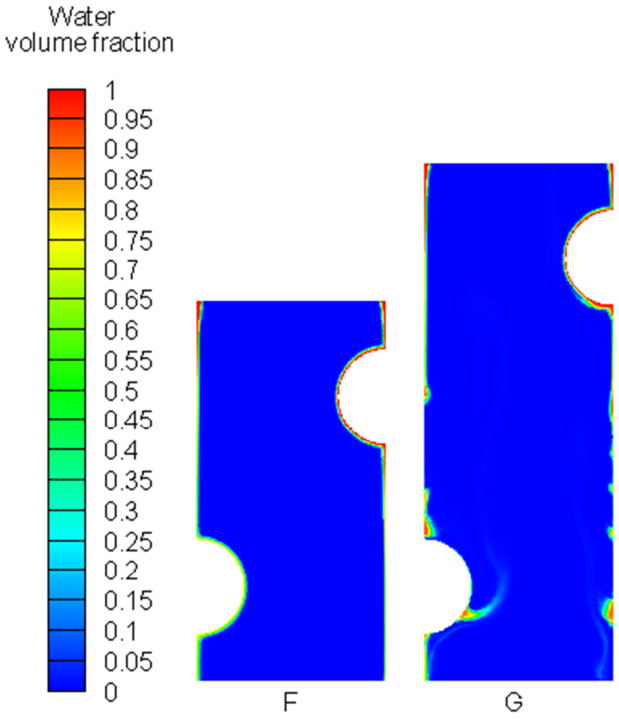

Figure 12. Influence of the tubes arrangement on the flow mode.

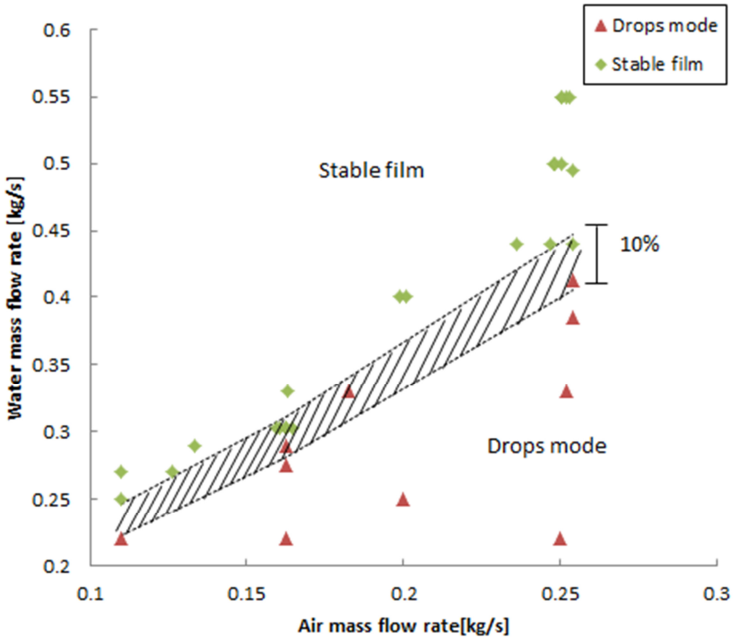

Figure 13. Trade off curve.

Tables

Table 1. Geometrical parameters of the tube banks.

d_{ext}	mm	25
P_l	mm	50
P_t	mm	100

Table 2. Results for the grid independence test.

	Grid 1	Grid 2	Grid 3
Water film thickness at θ=90°, (mm)	0.9384	0.9236	0.9016

Table 3. Grid details.

Grid characteristics	
Elements number	24510
Elements type	Triangular
Mesh scheme	Pave
Size function	
Start size	0.25
Growth rate	1.1
Maximum size	1
Boundary layers	
First row	0.15
Growth factor	1
Rows	20

Table 4. Simulation settings.

Space and time	2D, Unsteady
Solver	Segregated implicit
Model	Volume of Fluid
Species transport	Enabled
Material	Moist air (primary) Water (secondary)
Pressure-Velocity Coupling	SIMPLE
Gravitational Acceleration	-9.81 m/s^2
VOF Discretization Scheme	Geo-Reconstruct
Discretization pressure	PRESTO
Discretization momentum	First Order Upwind
Turbulence model	Standard k-ε

Table 5. Working fluid mass flow rates for the different testing cases.

	Unit	Air mass flow rate	Water mass flow rate
Testing case A	kg/s	0.25	0.55
Testing case B	kg/s	0.25	0.44
Testing case C	kg/s	0.25	0.33
Testing case D	kg/s	0.16	0.33
Testing case E	kg/s	0.16	0.25

Table 6. Simulations settings and geometrical parameters.

Air mass flow rate	kg/s	0.165
Water mass flow rate	kg/s	0.302
Outside tube diameter	mm	25
Transversal pitch	mm	100
	Longitudinal pitch	
Testing case F	mm	50
Testing case G	mm	86.6

Table 7. Fluids mass flow rates for the different cases.

N.	Air mass flow rate [kg/s]	Water mass flow rate [kg/s]	N.	Air mass flow rate [kg/s]	Water mass flow rate [kg/s]
1	0.248	0.11	**17**	0.163	0.33
2	0.1623	0.22	**18**	0.1826	0.33
3	0.25	0.22	**19**	0.252	0.33
4	0.11	0.22	**20**	0.254	0.385
5	0.11	0.25	**21**	0.199	0.4
6	0.2	0.25	**22**	0.20109	0.4
7	0.11	0.27	**23**	0.254	0.4125
8	0.12641	0.27	**24**	0.2364	0.44
9	0.1623	0.275	**25**	0.247	0.44
10	0.13364	0.29	**26**	0.254	0.44
11	0.1623	0.29	**27**	0.254	0.495
12	0.15967	0.3025	**28**	0.248	0.5
13	0.1604	0.3025	**29**	0.25035	0.5
14	0.1624	0.3025	**30**	0.25055	0.55
15	0.1626	0.3025	**31**	0.252	0.55
16	0.16436	0.3025	**32**	0.25313	0.55

References

[1] M.C. Chyu and A.E. Bergles. An analytical and experimental study of falling film evaporation on a horizontal tube. *ASME J. Heat Transfer*, 109(4):983–990, 1987.

[2] J. T. Rogers. Laminar falling film flow and heat transfer characteristics on horizontal tubes. *The Canadian Journal of Chemical Engineering*, 59(2):213–222, 1981.

[3] J. T. Rogers and S. S. Goindi. Experimental laminar falling film heat transfer coefficients on a large diameter horizontal tube. *The Canadian Journal of Chemical Engineering*, 67(4):560–568, 1989.

[4] R. Armbruster and J. Mitrovic. Patterns of falling film flow over horizontal smooth tubes. In *Proceedings of the Tenth International Heat Transfer Conference*, volume 3, pages 275–280, 1994.

[5] X. Hu and A.M. Jacobi. The intertube falling film part 1 - flow characteristics mode transitions and hysteresis.',. *ASME J. Heat Transfer*, 118:616–625, 1996.

[6] D. Yung, J.J. Lorentz, and E.N. Ganic. Vapor/liquid interface and entrainment in falling film evaporators. *Journal of Heat Transfer*, 102:20–25, 1980.

[7] H. Honda, S. Nozu, and Y. Takeda. Flow characteristics of condensation on a vertical column of horizontal tubes. In *ASME - JSME Thermal Engineering Joint Conference*, volume 1, Honolulu, 1987.

[8] R.O. Parker and R.E. Treybal. The heat mass transfer characteristics of evaporative coolers. *Chemical Engineering Progress Symposium Series*, 57(32):138–149, 1961

[9] T. Mizushina, R. Ito, and H. Miyashita. Experimental study of an evaporative cooler. *International Chemical Engineering*, 7(4):727–732, 1967

[10] D.K. Kreid, B.M. Johnson, and D.W Faletti. Approximate analysis of heat transfer from the surface of a wet finned heat exchanger. *ASME*, (78HT-26.), 1978.

[11] W. Leidenfrost and B. Korenic. Evaporative cooling and heat transfer augmentation related to reduced condenser temperature. *Heat Transfer Engineering*, 3:38–59, 1982.

[12] A.V. Bykov, V.A Gogolin, and N.V. Tovaras. Investigation of heat, mass transfer and fluid flow characteristics in evaporative condensers. *International Journal of Refrigeration*, 7(6):342–347, 1984.

[13] R.L. Webb. A unified theoretical treatment for thermal analysis of cooling towers, evaporative condensers and fluid coolers. In *ASHRAE Transaction*, volume 90, pages 398–415, Kansas City, 1984.

[14] P. J. Erens and A. A. Dreyer. An improved procedure for calculating the performance of evaporative closed circuit coolers. In *Proc. 25th National Heat Transfer Conference*, volume 84 of *American Institute of Chemical Engineers Symposium Series*, pages 140–145, Houston, 1988.

[15] W. Zalewski and P.A. Gryglaszewski. Mathematical model of heat and mass transfer processes in evaporative fluid coolers. *Chemical Engineering and Processing: Process Intensification*, 36(4):271–280, 1997.

[16] M. Poppe and H. Rögener. Evaporative cooling systems. *VDI-Wärmeatlas*, pages pp. Mh1–Mh15, 1984.

[17] F. Bosnjakovic. *Technical Thermodynamics*. New York, 1965

[18] H.M. Ettouney, H.T. El-Dessouky, W. Bouhamra, and B. Al-Azmi. Performance of evaporative condensers. *Heat Transfer Engineering*, 22(4):41–55, 2001.

[19] B.A. Qureshi and S.M Zubair. A comprehensive design and rating study of evaporative coolers and condensers. part i. performance evaluation. *International Journal of Refrigeration*, 29(4):645–658, 2006.

[20] B.A. Qureshi and S.M. Zubair. Prediction of evaporation losses in evaporative fluid coolers. *Applied Thermal Engineering*, 27(2-3):520–527, 2007.

[21] K.A. Jahangeer, A.A.O. Tay, and M.R. Islam. Numerical investigation of transfer coefficients of an evaporatively-cooled condenser. *Applied Thermal Engineering*,31(10):1655–1663, 2011.

[22] M. Fiorentino and G. Starace. A numerical model to investigate evaporative condensers behavior at tube scale. In *ASME 2014 – 12th Biennial Conference on Engineering Systems and Analysis,* American Society of Mechanical Engineering, 2014.

[23] M.R. Islam, K.A. Jahangeer, K.J. Chua. Experimental and numerical study of an evaporatively-cooled condenser of air-conditioning systems. *Energy*,87:390-399, 2015.

[24] *Heat Exchanger Design Handbook*, Hemisphere Publishing Corporation. New York, 1983.

[25] R.E. Bolz and G.L. Tuve. *CRC Handbook of Tables for Applied Engineering Science. 2nd Edition*. CRC Press, 1973.

[26] F. Jafar, G. Thorpe, and O.F. Turan. Liquid film falling on horizontal circular cylinders. pages 1193–1200, Gold Coast, Queensland, Australia, December 2007.

[27] M. Thiruvengadam, B. F. Armaly, and J. A. Drallmeier. Shear-driven liquid film in a duct. *Engineering Applications of Computational Fluid Mechanics*, 3(4):506–513, 2009.